An analysis and preliminary experiment of the discharge characteristics of RF ion source with electromagnetic shielding

Na WANG (王娜)[1,2] , **Zhimin LIU** (刘智民)[1,2], **Yahong XIE** (谢亚红)[1,2,*] ,
Jianglong WEI (韦江龙)[1] , **Caichao JIANG** (蒋才超)[1,2], **Wei LIU** (刘伟)[1],
Xufeng PENG (彭旭峰)[1,2], **Guojian SU** (苏国建)[1] and **Junwei XIE** (谢俊炜)[1,2]

[1] Institute of Plasma Physics, Hefei Institutes of Physical Science, Chinese Academy of Sciences, Hefei 230031, People's Republic of China
[2] University of Science and Technology of China, Hefei 230026, People's Republic of China

E-mail: xieyh@ipp.ac.cn

Abstract
Combined with two-dimensional (2D) and three-dimensional (3D) finite element analysis and preliminary experimental tests, the effects of size and placement of the electromagnetic shield of the radio-frequency (RF) ion source with two drivers on plasma parameters and RF power transfer efficiency are analyzed. It is found that the same input direction of the current is better for the RF ion source with multiple drivers. The electromagnetic shield (EMS) should be placed symmetrically around the drivers, which is beneficial for the plasma to distribute uniformly and symmetrically in both drivers. Furthermore, the bigger the EMS shield radius is the better generating a higher electron density. These results will be of guiding significance to the design of electromagnetic shielding for RF ion sources with a multi-driver.

Keywords: RF ion source, electromagnetic shielding, RF transfer efficiency

(Some figures may appear in colour only in the online journal)

1. Introduction

The aim of the Comprehensive Research Facility for Fusion Technology (CRAFT) negative neutral beam injection (NNBI) system enables us to deliver a powerful beam with a beam energy of 200–400 keV, beam power of 2 MW, and beam duration of 100 s [1–4]. To provide stalely such a high-power injection for a long experimental period without maintenance, a large-area radio-frequency (RF) ion source will be adopted for the neutral beam injection (NBI) system [5–8]. Due to the large extraction area of this ion source, a multiple driver structure will be used, each of which is powered separately by a 100 kW RF generator. Since the excitation current in the coil is alternating current, mutual inductive coupling tends to occur between the drivers, which affects the deposition of RF power in the plasma and leads to asymmetric plasma distribution in multiple drivers. It was found that inductive coupling is reduced by inserting a copper plate between adjacent drivers or surrounding each driver with copper shielding [9–11].

The RF ion source with two drivers was tested at the Institute of Plasma Physics, Chinese Academy of Sciences (ASIPP) test facility and was powered by a 100 kW RF generator for a pair of RF drivers connected in series. During the test of this RF ion source without an electromagnetic shield (EMS), the plasma luminous intensity was different in the two drivers as shown in figure 1. Additionally, stable discharge cannot be maintained. To balance and stabilize the discharge, the drivers were covered with a pair of cylindrical shaped EMSs made of copper. As a result, a long-pulse discharge was achieved for 1000 s at the RF power of 82 kW [12]. The placement and size of the copper EMS can affect the internal magnetic field distribution of the driver, which in turn affects the plasma distribution and RF power deposition.

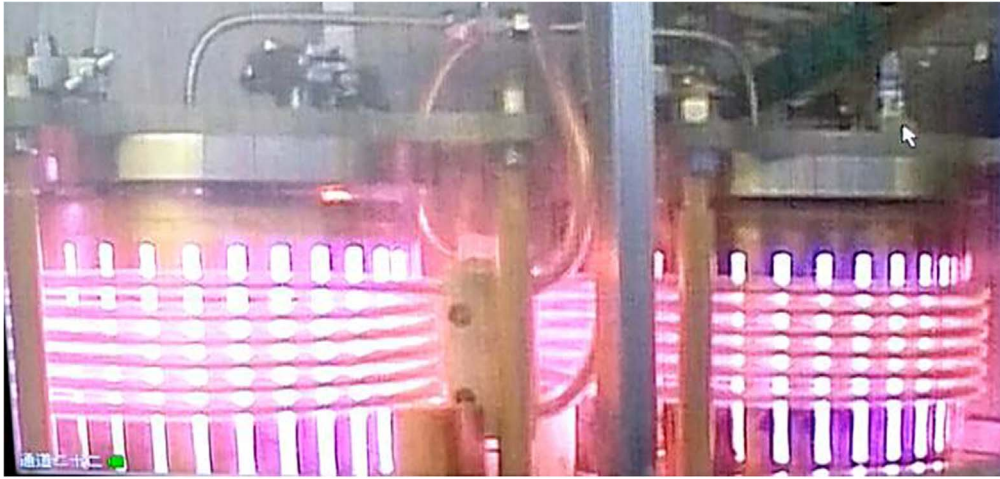
* Author to whom any correspondence should be addressed.

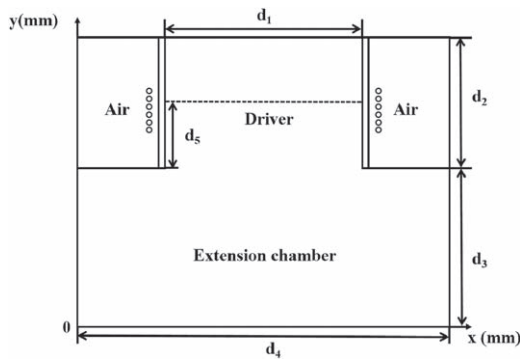**Figure 1.** Diagram of the RF ion source with two drivers discharge experiment.

Figure 2. Scheme of the 2D finite element model of RF ion source with a single driver.

Figure 3. Scheme of the 2D finite element model of RF ion source with two drivers.
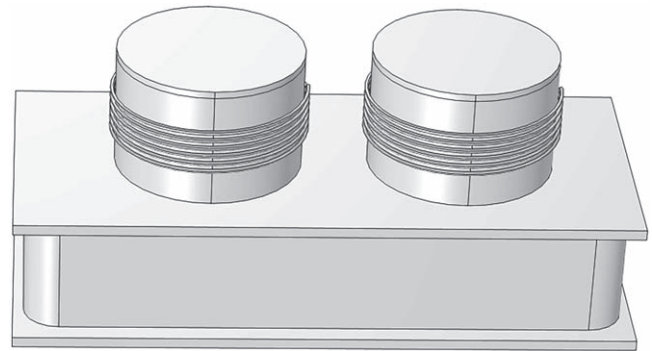
Figure 4. The schedule of the 3D finite element model of the RF ion source with two drivers.

To be suitable for the stable operation of the CRAFT NNBI multi-drive RF ion source in the future, a detailed study of the EMS between the RF drivers is required.

2. Method

2.1. Model introduction

Two kinds of finite element models were developed: a two-dimensional (2D) fluid model based on plasma discharge, and a three-dimensional (3D) electromagnetic model based on uniform conductivity analysis.

The 2D fluid model of the RF ion source is shown in figures 2 and 3, which illustrate the configurations of the driver, RF coil, an Al_2O_3 cylinder, and the plasma expansion chamber. The adjacent area between the two drivers is defined as region E. The dashed lines in figures 2 and 3 indicate the center positions of the drivers which are located 82.5 mm from the upper plate of the expansion chamber. The structural parameters of the 3D model of the RF ion source with two drivers shown in figure 4 remain the same as the 2D model. The 3D plasma discharge calculation is not involved in this study, so the model does not include the Faraday shield which is used to protect the Al_2O_3 cylinder and suppress capacitive
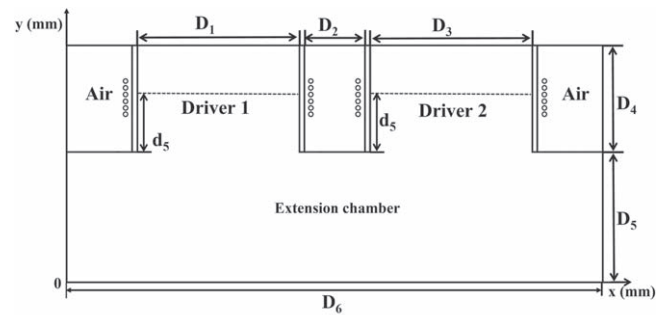
coupling [7, 13, 14]. The main structural parameters of these models are shown in table 1.

2.2. Initial conditions of the model

In the 2D fluid model, the discharge gas pressure is set as 2 Pa, the RF power is 20 kW, and the RF frequency is set as the typical value of 1 MHz [12, 15–19]. The frequency domain-transient study is used for calculations in the time range of 10^{-8}–10^{-4} s, with a calculated time step of $4/30$ s. The main atomic and molecular processes in the plasma taken into account are listed in table 2.

Table 1. Parameters of the models.

Parameters	Values
d_1	250
d_2	165
d_3	200
d_4	470
d_5	82.5
D_1	250
D_2	78
D_3	250
D_4	165
D_5	200
D_6	830

In the 3D model, the plasma is assumed to be a homogeneous conducting medium and the conductivity parameters are derived from the average electron density and electron temperature in the *x*-axis direction at the center position of the driver (where the dashed line is located in the figure 1) in the 2D model [24]. Since the Faraday shield structure cannot be considered in the 2D model, the electron density would be overestimated. Meanwhile, the electron density in the expansion chamber is lower than that in the driver, which leads to a too-high calculated conductivity. However, as a qualitative study of the EMS placement, this overestimation does not affect the trend of the results.

2.3. Thesis of the model

2.3.1. Thesis of the 2D model.
The equation for the electron density is given by [25, 26]:

$$\frac{\partial n_e}{\partial t} + \nabla \cdot \mathbf{\Gamma}_e = R_e - (\boldsymbol{u} \cdot \nabla)n_e, \tag{1}$$

where R_e is the electron rate expression in the dimension of $(m^3 \cdot s)^{-1}$, n_e is the electron density, $\boldsymbol{u}$ is the neutral fluid velocity vector, $\mathbf{\Gamma}_e$ is the electron flux vector given by:

$$\mathbf{\Gamma}_e = -(\mu_e \cdot \boldsymbol{E})n_e - \nabla(\boldsymbol{D}_e n_e), \tag{2}$$

where $\boldsymbol{E}$ is the electric field (unit: V m^{-1}), the $\boldsymbol{D}_e$ is the electron diffusivity (unit: m^2 s^{-1}), the e refers to an electron, the μ_e is the electron mobility (unit: m^2 (V·s)$^{-1}$).

The electron energy density is given by the following equation:

$$\frac{\partial n_\varepsilon}{\partial t} + \nabla \cdot \mathbf{\Gamma}_\varepsilon + \boldsymbol{E} \cdot \mathbf{\Gamma}_e = S_{en} - (\boldsymbol{u} \cdot \nabla)n_\varepsilon + \frac{(Q + Q_{gen})}{q}, \tag{3}$$

$$\mathbf{\Gamma}_\varepsilon = -(\mu_\varepsilon \cdot \boldsymbol{E})n_\varepsilon - \nabla(\boldsymbol{D}_\varepsilon n_\varepsilon), \tag{4}$$

where n_ε is the electron energy density (unit: V m^{-3}), S_{en} is the energy loss or gain due to inelastic collisions (unit: V (m^3·s)$^{-1}$), Q is an external heat source (unit: W m^{-3}), Q_{gen} is a generalized heat source (unit: W m^{-3}), μ_ε is the electron energy mobility (unit: m^2 (V·s)$^{-1}$), $\boldsymbol{D}_\varepsilon$ is the electron energy diffusivity (unit: m^2 s^{-1}), the ε refers to electron energy (unit: eV) [26].

The electrostatic field is given as:

$$\nabla \cdot (\varepsilon_0 \varepsilon_r \boldsymbol{E}) = \rho_q, \tag{5}$$

where the ρ_q is space charge density (unit: C m^{-3}), the ε_r is the relative permittivity, the ε_0 is the permittivity of vacuum, the velocity of an electromagnetic wave in a vacuum is given as c_0 and the permittivity of a vacuum is derived from the relation:

$$\varepsilon_0 = \frac{1}{c_0^2 \mu_0} \approx 8.854 \times 10^{-12} \, \text{F m}^{-1}.$$

The electric potential V is defined by the following equation:

$$\boldsymbol{E} = -\nabla V. \tag{6}$$

The cross-section data is used to define source coefficients in the model, and a Maxwellian electron energy distribution function (EEDF) is assumed as the following formula [27]:

$$f(\varepsilon) = \Phi^{-\frac{3}{2}} \beta_1 \exp\left(-\left(\frac{\varepsilon \beta_2}{\Phi}\right)\right), \tag{7}$$

where

$$\beta_1 = \Gamma\left(\frac{5}{2}\right)^{\frac{3}{2}} \Gamma\left(\frac{3}{2}\right)^{-\frac{5}{2}}, \tag{8}$$

$$\beta_2 = \Gamma\left(\frac{5}{2}\right) \Gamma\left(\frac{3}{2}\right)^{-1}, \tag{9}$$

where Φ is the mean electron energy (unit: eV), and the Γ is the incomplete gamma function:

$$\Gamma(s) = \int_0^\infty u^{s-1} e^{-u} du. \tag{10}$$

2.3.2. Thesis of the 3D model.
The 3D model is solved in the frequency domain, and follows Ampère's law including displacement currents as formulas (11) and (12):

$$\nabla \times \boldsymbol{H} = \boldsymbol{J}, \tag{11}$$

$$\boldsymbol{J} = \sigma \boldsymbol{E} + j\omega \boldsymbol{D} + \sigma \boldsymbol{v} \times \boldsymbol{B} + \boldsymbol{J}_e, \tag{12}$$

where $\boldsymbol{H}$ is the magnetic field intensity, $\boldsymbol{B}$ is magnetic flux density, σ is the electrical conductivity, $\boldsymbol{J}_e$ is an externally generated current, $\boldsymbol{v}$ is the velocity of the conductor, and $\boldsymbol{D}$ is electric flux density.

The definitions of the fields are as formulas (13) and (14):

$$\boldsymbol{B} = \nabla \times \boldsymbol{A}, \tag{13}$$

$$\boldsymbol{E} = -j\omega \boldsymbol{A}, \tag{14}$$

where $\boldsymbol{A}$ is magnetic vector potential.

Table 2. The gas-phase reactions considered in this work.

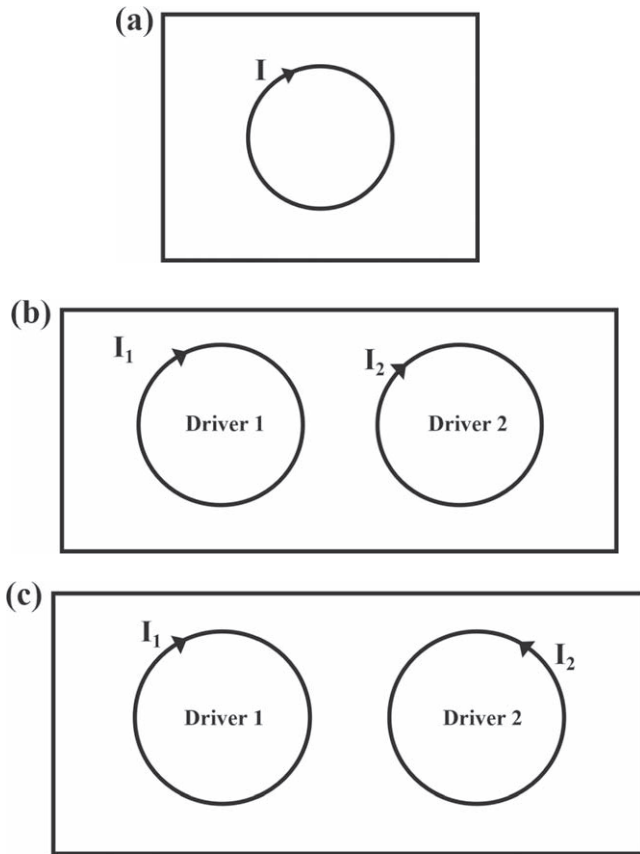| Gas-phase reactions	Description	Threshold energy (eV)	References
$e + H = H^+ + 2e$	Ionization	13.6	[20, 21]
$e + H_2^+ = H^+ + H + e$	Dissociative excitation	12.4	[20, 22]
$e + H_2 = H^+ + H + 2e$	Dissociative ionization	18	[20, 22]
$e + H_2 = H_2^+ + 2e$	Molecular ionization	15.4	[20, 23]
$H_3^+ + e = H + H + H$	Dissociative recombination	0	[20, 22]
$H_2 + e = e + H + H$	Dissociation	8.8	[20, 22]
$H_2 + e = e + H_2$	Elastic scattering		[20, 22]

Figure 5. Current direction in the top view of: (a) RF ion source with a single driver, (b) RF ion source with two drivers, (c) RF ion source with two drivers.

Figure 6. Comparison of electron density between the RF ion source with a single driver and two drivers (with the same current and reverse current respectively).

3. Results and discussion

3.1. Parameter analysis of the RF driver without EMS

The current feed direction of coils with single and two drivers are shown in figure 5. The distributions of electron density and electron temperature along the dashed line crossing the two drivers in figure 3 are shown in H–L and H–R in figure 6. The curve with the symbol 'S' in figure 6 indicates the distribution of electron density at the same position in the RF ion source with a single driver. As can be seen from figure 6, the mutual inductive coupling between the multiple RF drivers causes the electron density distribution in the drivers to change. The positions of peak electron density in both drivers are offset from the 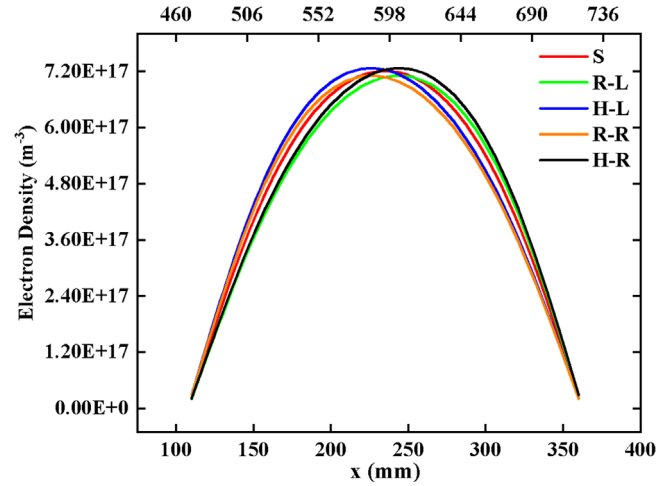center and move to the side away from the adjacent coils. The peak in the left driver deviates to the left, and in the right driver, it deviates to the right. Meanwhile, the maximum electron density of two drivers is larger than that of the single driver. When the reverse current is fed into the two coils as shown in figure 5(c), the electron density distributions are shown as lines R–L and R–R in figure 6. In the peak positions appears a similar phenomenon, but the deviation is opposite to the case of figure 5(b), i.e., the peak in the left driver deviates to the right, and in the right driver, it is reversed. The value of electron density is slightly decreased compared to that of a single driver. This phenomenon is mainly due to the electromagnetic coupling between the drivers making the magnetic field generated by the RF coils distributed asymmetrically in the drivers.

Figure 7(a) shows the magnetic field distribution between two drivers fed with the same currents at $T = 1.35 \times 10^8$ s (before the plasma is established). It indicates an obvious mutual inductive coupling phenomenon between the drivers. While the magnetic field distribution in figure 7(b) is obtained by feeding reverse currents in the two drivers. It shows a magnetic field 'hole' between the drivers, because of the canceling effect of the magnetic fields generated by the currents of the two driver coils flowing in opposite directions. However, this cancellation does not completely cover the entire adjacent area. There is still obvious interaction between the coils.
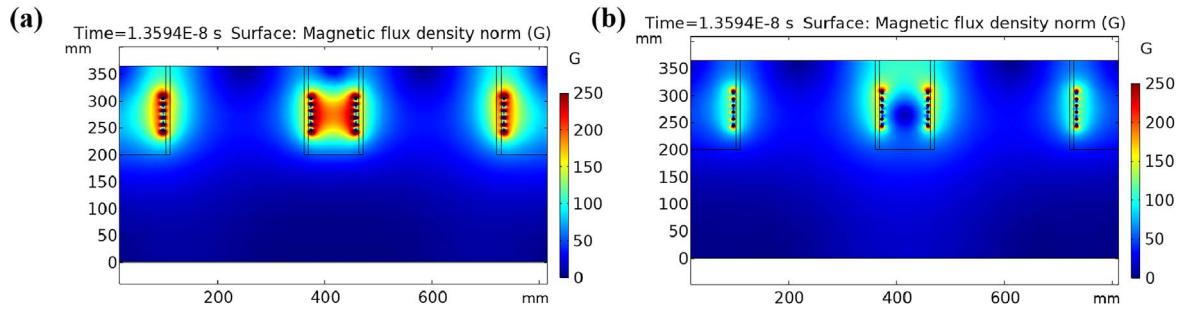
Figure 7. Magnetic field distributions of the RF source with two drivers. (a) Fed with the same current, (b) fed with the reverse currents.
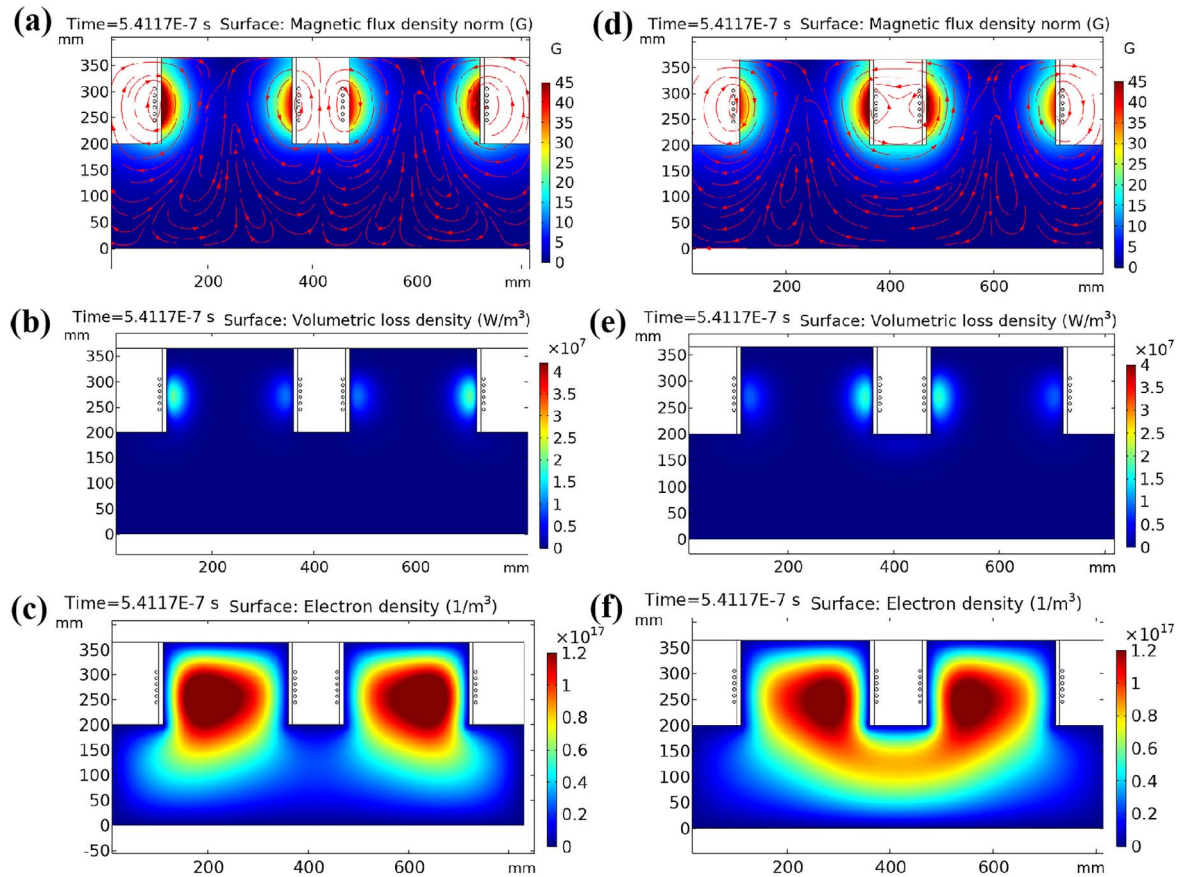

Figure 8. RF ion source fed with the same current: (a) magnetic field distribution, (b) RF power deposition distribution, (c) electron density distribution. RF ion source fed with the reverse current: (d) magnetic field distribution, (e) RF power deposition distribution, (f) electron density distribution.

The electron density distribution, magnetic field distribution, and power deposition distribution were calculated at the time of $T = 5.4117 \times 10^7$ s (early plasma build-up during the discharge process). The magnetic field energy inside the driver is concentrated in the edge region of the plasma and does not reach the core due to the presence of the RF sheath. As depicted in figures 8(a) and (d), in the dual-driver RF ion source fed with the same current, the magnetic field near the edge on the adjacent coil side is weaker than that at the edge away from the adjacent coil. That is because the magnetic field inside the drivers near region E weakens each other. For the RF ion source fed with reverse currents, the distribution of the magnetic field strength is opposite to the former. Furthermore, as shown in figures 8(b) and (e) for the power

deposition distribution in both ion sources, the region where the power is mainly deposited corresponds to the region with the higher magnetic field strength in figures 8(a) and (d). This asymmetric distribution of power supports the above explanation for the difference in electron density distribution in figure 6. Figures 8(c) and (f) show the effects of currents in different input directions in the coil on the distribution of the electron density. Compared to the magnetic field distribution of ion source with one driver, the magnetic field interaction between the dual drivers causes an asymmetry in the magnetic field energy at the left and right inner edges in each driver, with the position of the maximum value of the electron density biased towards the side of the larger value of power deposition.
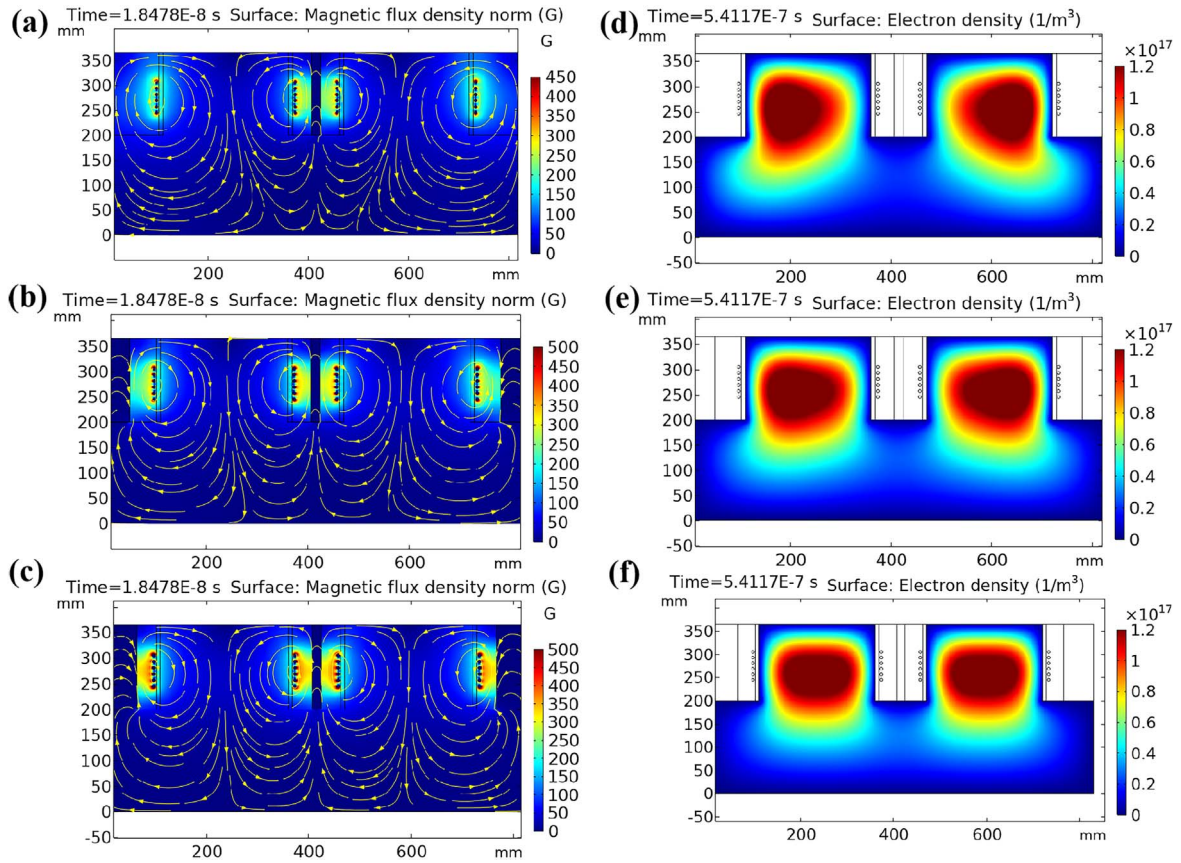
Figure 9. Magnetic field distributions in the driver: (a) with single-side EMS, (b) with asymmetric EMS, (c) with symmetric EMS. Electron density distributions in the driver: (d) with single-side EMS, (e) with asymmetric EMS, (f) with symmetric EMS.

3.2. Analysis of the influence of EMS position on driver parameter

3.2.1. Exploration of EMS placement symmetry. An attempt is made to place an EMS in the region E [9], and the distribution of the electromagnetic field and electron density in the driver with different positions of the EMS is shown in figure 9. It is found that when the EMS is placed asymmetrically as shown in figures 9(a) and (b), it leads to an uneven distribution of electron density in the driver region (as shown in figures 9(d) and (e)). While in figure 9(c), both sides of the EMS are at equal distances from the outer wall of the Al_2O_3 cylinder and the electron density in the driver shows a uniform distribution as shown in figure 9(f). When the EMS is placed asymmetrically around the RF ion source, it makes the magnetic field energy around the coils on both sides 'leak out' differently. It causes the difference in RF magnetic field distribution pattern, thus leading to the different power deposition near the coil on both sides of the same driver. The position of the maximum electron density would shift, and the distribution of electron density would be uneven in the driver.

3.2.2. Effect of EMS radius on the electron density. As illustrated in figure 10 with RF power of 20 kW and pressure of 2 Pa, the electron density distributions in the driver with and without EMS are compared. The electron density is taken
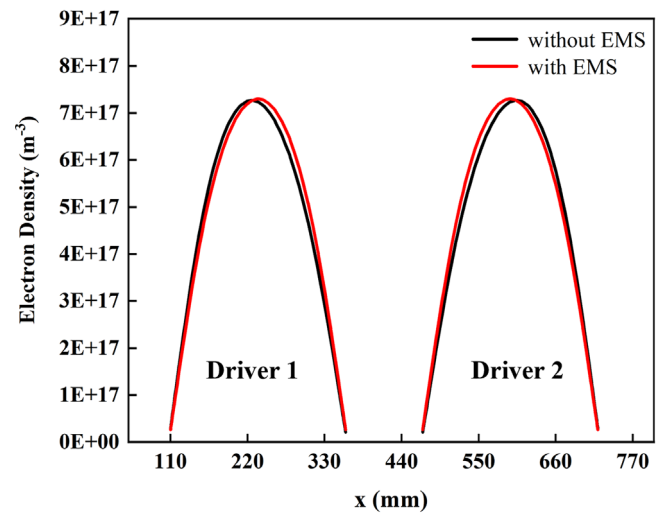

Figure 10. Comparison of electron density of two drivers with and without EMS.

from the center of the coil as described above, i.e., the dotted line at the distance of d_5 from the upper plate of the expansion chamber in figure 3. It was found that when EMS was added to the periphery of the driver, the electron density in the center of both drivers was slightly higher than that without EMS. When there is no EMS, the magnetic field generated by the coil is distributed in the space around the driver. While with the addition of EMS, the magnetic field is concentrated
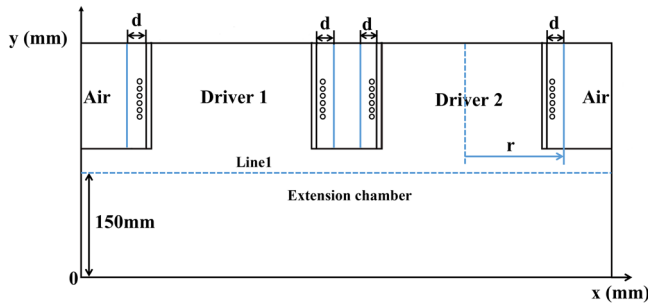
Figure 11. Scheme of the 2D finite element model of RF ion source with two drivers (with EMS).

near the coil, and the energy that can be coupled into the drive increases. Consequently, the electron density in the driver increases. As mentioned in section 3.1, when the electromagnetic shield is placed asymmetrically compared to the outer wall of the driver, this will cause the magnetic field energy coupled into the driver by the coils on both sides of the same driver to be different. As a result, the electron density is distributed asymmetrically in the ion source. The reason for the shift of the peak position has been explained in the previous section.

The radius of the EMS, illustrated by '*r*' in figure 11, is varied to research the changes in the shielding effect. The '*d*' in figure 11 represents the distance from the inner wall of the EMS to the outer wall of the Al$_2$O$_3$ cylinder of the driver, and it is used instead of *r* to change the configuration easier. The EMS radius in the following analysis refers to the value of *d*. Figure 12 depicts the variation of electron density in drivers with different radii of EMS. It is found that the electron density in the center of the driver increases with the increase of the radius of the EMS. When the value of *d* increases to 25 mm, the electron density hardly changes after continuing to increase the radius. In the RF ion source, the upper plate of the expansion chamber is not magnetically insulated, the magnetic field generated by the coil can pass through it. More magnetic field energy can penetrate the expansion chamber through the upper plate with the increase of the radius of EMS. Because the RF magnetic field energy is mainly concentrated near the coil, with the increase of the distance from the coil, the magnetic field strength will rapidly decay. After reaching a certain distance, and continuing to increase the radius, the increment of magnetic field energy that can be coupled into the ion source will be small. The magnetic field strength changes near the coil in the range of the horizontal coordinate (0–90 mm) are simulated. It is found that the absolute value of the change rate of magnetic field strength in the range of 0–30 mm is 1.47 while being about 0.1 in the range of 30–90 mm, which well supports the above explanation. This is why the difference in the variation of the electron density at the center of the driver gradually decreases by continuously varying the electromagnetic shielding radius with a length of 5 mm.

3.2.3. Effect of EMS radius on RF transfer efficiency. The power loss in the driver cannot be calculated in the 2D fluid
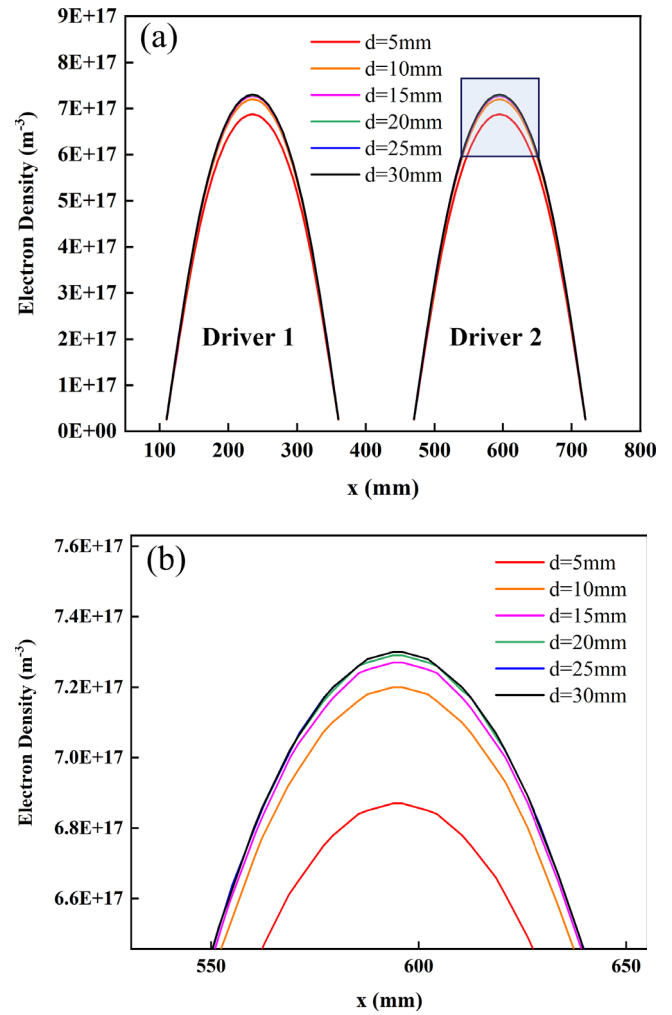

Figure 12. (a) Electron density comparison in drivers with EMS of different radii, (b) the local magnified diagram of the left graph.

model. Therefore, a 3D electromagnetic model is established to calculate the RF transfer efficiency under different EMS radii. In the model, the plasma is regarded as a uniform conductive substance. The electron density in the two drivers is calculated by the 2D fluid model. The line averaged values of electron density and electron temperature in the two drivers are calculated at the location shown by the dashed lines in figure 3. The plasma equivalent conductivity is calculated by these average values [24]. This conductivity is substituted into the 3D model as input. Among these calculation procedures, the coil current of the driver in the 3D model is also calculated from the 2D model with an RF power of 20 kW. When the Faraday shield is not considered in the model, most RF power would be deposited in the plasma. By calculating the power at both ends of the coil as the input power P_{coil} and calculating the power deposited in the plasma domain P_{plasma}, the RF transfer efficiency is given as:

$$\eta = \frac{P_{plasma}}{P_{coil}} \times 100\%. \qquad (15)$$

As depicted in figure 13, for the RF ion source with two drivers, the addition of the EMS increases the RF efficiency,
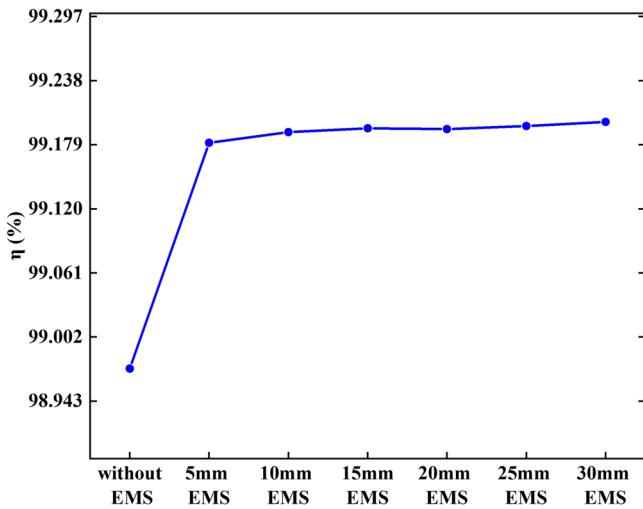
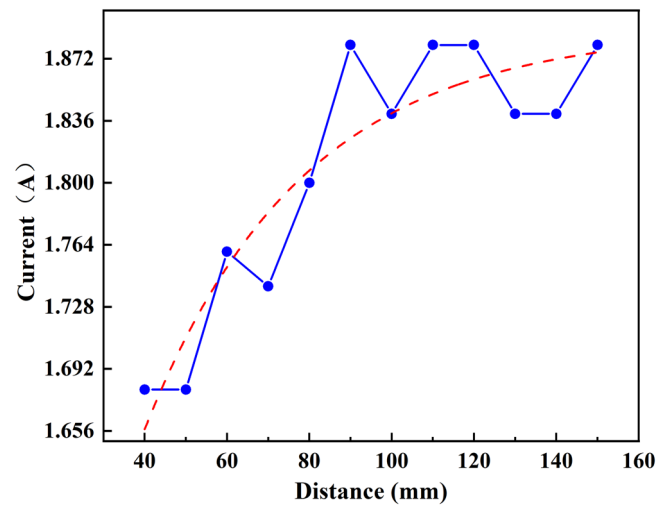**Figure 13.** RF transfer efficiency of the RF ion source with different EMS radii.

Figure 15. Variation of induced current with EMS radius in the coil without the generator.
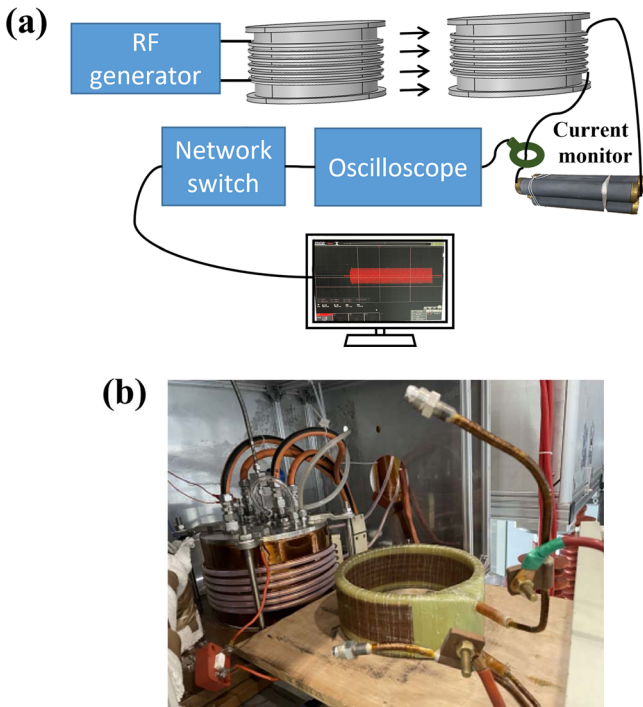

Figure 14. (a) Schematic diagram of the experiment, (b) experimental setup.

which raises with the increase of the EMS radius. Saturation tendency appears at the *d* of 15 mm in figure 13, the variation of the RF efficiency becomes smaller when continues to increase the electromagnetic shielding radius. This saturation characteristic is consistent with the change in electron density. An experiment was designed to measure the effect of different EMS radii on the induced currents in adjacent coils.

The experiment was conducted at the RF ion source test facility at ASIPP. Since the current experimental process is focused on testing the RF negative ion source with one driver, the induced current generated by the RF coil in the adjacent coils while performing the RF discharge was briefly explored. Figure 14 illustrates the diagram of the experiment, where a

coil without the generator is placed next to the RF driver. A resistor of 3.6 Ω is connected in series with the coil to simulate the change of the induced current in the presence of plasma. The oscilloscope (VDS6104 produced by OWON Company) is connected between the current monitor (Pearson 110) and the network switch. Then the RF current data is transmitted to the computer for acquisition.

The variation of current in the coil without a generator was measured. A quarter-circle shaped oxygen-free copper was added as the EMS between the coils. The distance between the outer wall of the RF driver and the unexcited coil is 168 mm. Under the RF power of 60 kW, the distance between the outer walls of the EMS and the RF driver is varied in the range of 40–150 mm. This distance is defined as the radius of the EMS. The results are shown in figure 15. The induction current in the unexcited coil shows an overall increasing trend as the EMS radius increases. This is because the magnetic field that can leak beyond the EMS raises as the radius of the EMS increases. During the measurement, the reflection coefficient of the RF power source is 1.9 when the EMS radius is 40 mm, and 1.05 when it is 50 mm. The reflection coefficient drops to about 0.6 when the radius is larger than 50 mm, which is so large that the RF ion source cannot operate normally. To obtain better plasma parameters and RF transfer efficiency, we suggested that the distance between the EMS and the outer wall of the RF ion source should be as large as possible while the size allows.

4. Conclusions

A 2D plasma discharge model and a 3D electromagnetic model of the RF ion source with two drivers were established. The effect of mutual inductance between the drivers on the electron density in the drivers is analyzed. When the input current direction in the two drivers is the same, the central electron density in the two drivers is toward the side away from the adjacent coil; when the input current direction in the

two drivers is reverse, the central electron density is deviated from the center of the driver and toward the side near the adjacent coil. Therefore, changing the direction of the input current in the coil does not eliminate the mutual inductive coupling between the two RF coils.

The use of a copper EMS can effectively shield the electromagnetic induction between the coils, but the position of the EMS needs to be symmetrically placed around the driver to make the plasma uniformly and symmetrically distributed in both drivers. The effect of the radius of the EMS on the plasma density in the driver was investigated. It is found that the electron density in the driver increased slightly with the EMS compared to that without it. The density increases initially and starts to saturate to the increase of the EMS radius. The average values of electron density and electron temperature at the middle position of the RF coil obtained in the 2D fluid model were used as input to the 3D model to calculate the RF conversion efficiency, and it was found that increasing the radius of the EMS could slightly increase the RF transfer efficiency. The dependency of the shielding effect for RF electromagnetic fields on the EMS radii was investigated experimentally. It was found that as the radius of EMS increases, the shielding effect on the mutual inductive coupling between the drivers becomes worse, but this mutual inductive coupling does not reduce the electron density in the drivers. A too small EMS radius increases the RF reflection. In the experiment, it is found that an electromagnetic shielding radius of less than 50 mm will produce a strong RF reflection. Therefore, it is recommended that the radius of the electromagnetic shield should be larger than 50 mm as much as possible when the size of the RF ion source allows.

Acknowledgments

ORCID iDs

Na WANG (王娜) ⓘ https://orcid.org/0000-0001-7005-2680
Yahong XIE (谢亚红) ⓘ https://orcid.org/0000-0002-1374-6544
Jianglong WEI (韦江龙) ⓘ https://orcid.org/0000-0002-2371-3842

References

[1] Xie Y H *et al* 2021 *Plasma Sci. Technol.* **23** 012001
[2] Wang N *et al* 2022 *Fusion Eng. Des.* **183** 113272
[3] Xie Y H *et al* 2021 *Fusion Eng. Des.* **167** 112377
[4] Wei J L *et al* 2021 *Fusion Eng. Des.* **169** 112482
[5] Wünderlich D *et al* 2021 *Nucl. Fusion* **61** 096023
[6] Wünderlich D *et al* 2019 *Nucl. Fusion* **59** 084001
[7] Kraus W *et al* 2008 *Rev. Sci. Instrum.* **79** 02C108
[8] Maistrello A *et al* 2021 *Fusion Eng. Des.* **167** 112337
[9] Kraus W *et al* 2012 *Rev. Sci. Instrum.* **83** 02B104
[10] Jain P *et al* 2022 *Plasma Phys. Control. Fusion* **64** 095018
[11] Kraus W *et al* 2018 *Rev. Sci. Instrum.* **89** 052102
[12] Xie Y H *et al* 2019 *Rev. Sci. Instrum.* **90** 113319
[13] Hopwood J 1994 *Plasma Sources Sci. Technol.* **3** 460
[14] Rauner D *et al* 2022 *Plasma* **5** 280
[15] Fantz U *et al* 2007 *Plasma Phys. Control. Fusion* **49** B563
[16] Kraus W *et al* 2015 *Fusion Eng. Des.* **91** 16
[17] Heinemann B *et al* 2017 *New J. Phys.* **19** 015001
[18] Bandyopadhyay M *et al* 2011 Two RF driver based negative ion source for fusion R&D *IEEE/NPSS 24th Symp. on Fusion Engineering (Chicago)* (IEEE) 1
[19] Jain P *et al* 2018 *Plasma Phys. Control. Fusion* **60** 045007
[20] Janev R K, Reiter D and Samm U 2003 *Collision Processes in Low-Temperature Hydrogen Plasmas* Report Jül-4105 Forschungszentrum Jülich
[21] Wang Y J *et al* 2021 *Chin. Phys.* B **30** 095205
[22] Zielke D 2021 Development of a predictive self-consistent fluid model for optimizing inductive RF coupling of powerful negative hydrogen ion sources *PhD Thesis* University of Augsburg, Augsburg, Germany
[23] Pitchford L C *et al* 2017 *Plasma Process. Polym.* **14** 1600098
[24] Grudiev A *et al* 2014 *Rev. Sci. Instrum.* **85** 02B134
[25] Hagelaar G J M and Pitchford L C 2005 *Plasma Sources Sci. Technol.* **14** 722
[26] Gogolides E and Sawin H H 1992 *J. Appl. Phys.* **72** 3971
[27] Dutton J 1975 *J. Phys. Chem. Ref. Data* **4** 577